ACS SENSORS

pubs.acs.org/acssensors
Article

High-Performance Piezoelectric Micro Diaphragm Hydrogen Sensor

Jihang Liu,* Doris Keh Ting Ng, Yul Koh, Subhranu Samanta, Weiguo Chen, Md Hazwani Khairy Md Husni, Merugu Srinivas, Qingxin Zhang, Fuu Ming Kai, Peter Hyun Kee Chang, and Yao Zhu*

Cite This: *ACS Sens.* 2025, 10, 1922−1929
Read Online

ACCESS | Metrics & More | Article Recommendations

ABSTRACT: Highly sensitive, selective, and compact hydrogen (H_2) sensors for safety and process monitoring are needed due to the growing adoption of H_2 as a clean energy carrier. Current resonant frequency-based H_2 sensors face a critical challenge in simultaneously achieving high sensitivity, low operating frequency, and miniaturization while maintaining a high figure of merit (FOM). This study addresses these challenges by introducing a novel piezoelectric micro diagram (PMD) H_2 sensor that achieves an unprecedented FOM exceeding 10^4. The sensor uniquely integrates a PMD resonator with a palladium (Pd) sensing layer, operating on a stress-based mechanism distinct from traditional mass-loading principles. Despite a low operating frequency of 150 kHz, the sensor demonstrates a remarkable sensitivity of 18.5 kHz/% H_2. Comprehensive characterization also reveals a minimal cross-sensitivity to humidity and common gases and a compact form factor (600 μm lateral length) suitable for IC integration. The sensor's performance was systematically evaluated across various Pd thicknesses (40−125 nm) and piezoelectric stack covering ratios (50% and 70%), revealing a trade-off between sensitivity and response time. This PMD H_2 sensor represents a significant advancement in resonant frequency-based H_2 sensing, offering superior sensitivity, compact size, and robust performance for diverse applications in H_2 detection and monitoring.

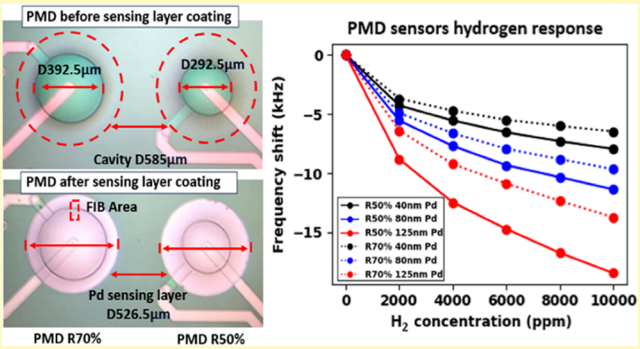

KEYWORDS: *piezoelectric micro diaphragm, palladium sensing layer, hydrogen sensor, resonant gas sensor, response stress-based*

The rising prominence of H_2 as a clean energy source has heightened the demand for accurate H_2 sensors, particularly for low-concentration leak detection. These sensors play a crucial role in safety applications across various industries, from automotive to aerospace.[1] The ability to detect H_2 at levels well below its lower flammable limit (4% in air) is essential for preventing potential hazards,[2] especially in confined spaces where even small leaks can accumulate to dangerous concentrations. Consequently, the development of sensitive and reliable H_2 sensors for low-concentration detection has become a priority impacting various aspects of modern life and technology.

Among various H_2 sensing technologies, resonant frequency-based sensors offer several distinct advantages. These sensors exhibit high sensitivity and rapid response times,[3] crucial for early leak detection. Unlike conventional electrical sensors, they are immune to electrical parasitic effects, enhancing reliability in diverse environments.[4] Resonant frequency-based H_2 sensors operate effectively at room temperature, eliminating the need for energy-intensive heating elements. This feature, combined with their inherently low power consumption, makes them ideal for portable and long-term monitoring applications.[5] Furthermore, their potential for miniaturization aligns well with the trend toward compact, integrated sensing systems.[6] These merits position resonant frequency-based H_2 sensors as a promising solution for addressing the growing demand for efficient and reliable hydrogen detection across various sectors.

Resonant frequency-based H_2 sensors consist of two main functional components: a resonator and a sensing layer. The resonator provides an electromechanical coupling signal with specific frequencies, while the sensing layer is responsible for H_2 absorption and desorption. This design features high flexibility in various applications, with overall performance dependent on both components. Examples of resonators include film bulk acoustic resonators (FBAR), surface acoustic wave (SAW) devices, and quartz crystal microbalances (QCM), operating at frequencies ranging from GHz to

Received: November 1, 2024
Revised: December 27, 2024
Accepted: February 13, 2025
Published: March 13, 2025

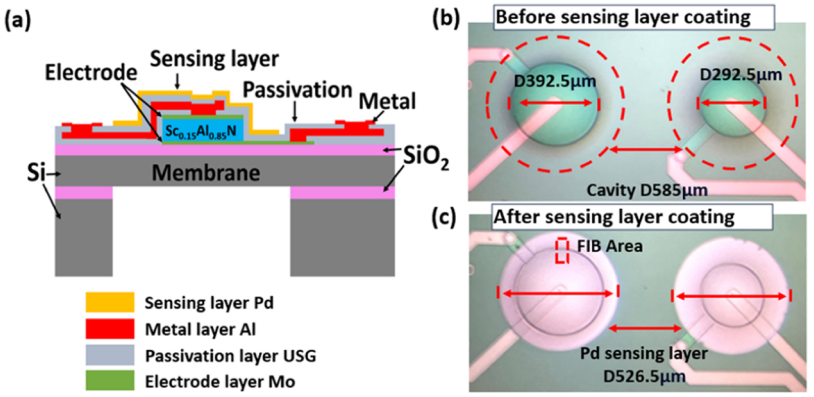

Figure 1. (a) Cross section view of PMD sensors. (b) Top view of PMD sensors before and (c) after the Pd coating.

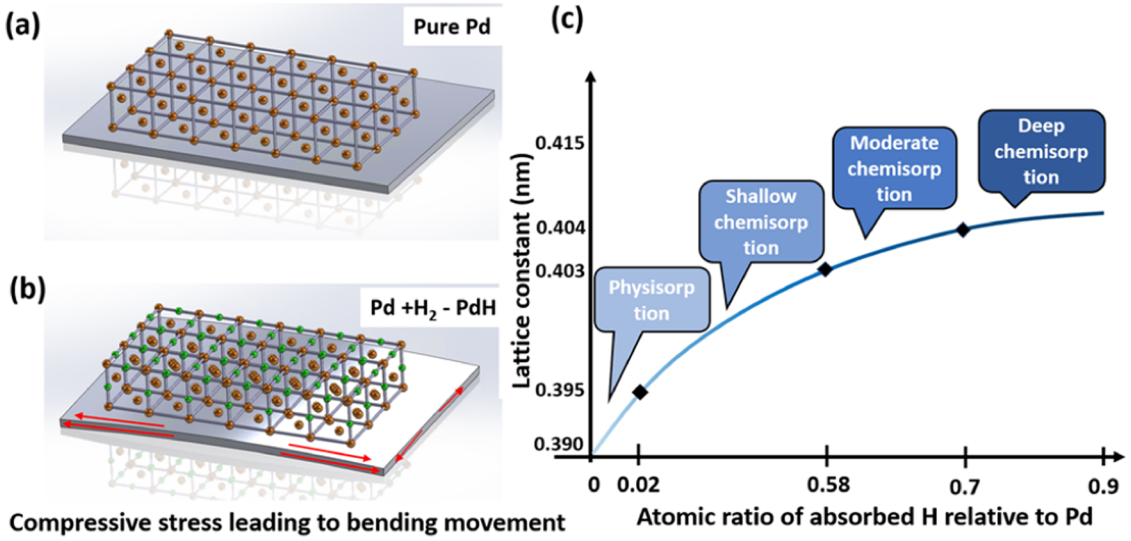

Figure 2. Schematics of Pd−H_2 reaction progress: (a) Pure Pd film lattice attached on substrate, (b) PdH_x and Pd composite film lattice during H_2 absorption, (c) PdH_x and Pd composite file lattice constant during H_2 absorption.

MHz.[6−12] Sensing layers typically utilize materials such as Pd, platinum (Pt), zinc oxide (ZnO), and its corresponding alloys or nanostructures.[7−15]

Recent studies have demonstrated the diverse capabilities of resonant frequency-based H_2 sensors, highlighting their potential for various applications. FBAR H_2 sensors excel in miniaturization and sensitivity. With a compact size of approximately 500 μm in lateral length, they achieve remarkable sensitivities: 5 MHz/% for 0−2% H_2 detection using Pd layer at 2.2 GHz, and 6 MHz/% for 0−3% H_2 detection using ZnO layer at 2.3 GHz.[7,8] SAW sensors, while larger (>3000 μm lateral length), offer a range of sensitivities. These span from 1.5 kHz/% with a Pd/Cu layer at 150 MHz to 55 kHz/% with a Pd/ZnO layer at 129 MHz, both for 0−1% H_2 detection.[9,10] QCM sensors present an intermediate size (>1800 μm) and varied performance: from 2.5 × 10^{-3} kHz/% for 2−20% H_2 detection using graphitic carbon nitride (g-C_3N_4) at 9 MHz, to 5.3 kHz/% for 0−0.025% H_2 detection with Pd at 165 MHz.[11,12]

Despite the advancements in resonant frequency-based H_2 sensors, they still face a key challenge in optimizing their FOM, defined as the ratio of sensitivity to eigenfrequency.[16,17] While higher sensitivity improves detection resolution, it often requires increased eigenfrequency according to the Sauerbrey mass equation,[7−12] which in turn demands more sophisticated interface circuits to mitigate noise issues. FBAR sensors currently lead with FOM levels of 10^3, followed by SAW sensors at 10^2, and QCM sensors at 10^1. The field urgently requires sensors with higher FOM values to enhance sensitivity without compromising performance or increasing circuit complexity. This necessitates innovative approaches in sensor design and material selection to advance H_2 detection capabilities.

This work introduces a novel H_2 sensing approach aimed at achieving an unprecedented FOM of 1 × 10^4 or higher. The key innovation lies in the unique integration of a PMD resonator with a Pd sensing layer, a combination unexplored in previous H_2 sensor research. This design leverages the PMD's flexible vibration mode, characterized by a low eigenfrequency (in hundred kHz range), and its exceptional frequency sensitivity to structural stress changes.[17,18] This stress-based mechanism, fundamentally different from Sauerbrey mass-loading principle, when combined with Pd's superior H_2 absorption properties, promises to dramatically enhance the H_2 sensor performance. The concept's viability was verified through theoretical analysis, finite element method (FEM) simulations, and comprehensive experimental validation, including sensor structure characterizations, H_2 response sensitivity/time tests, and cross-sensitivity analysis.

https://doi.org/10.1021/acssensors.4c03069
ACS Sens. 2025, 10, 1922−1929

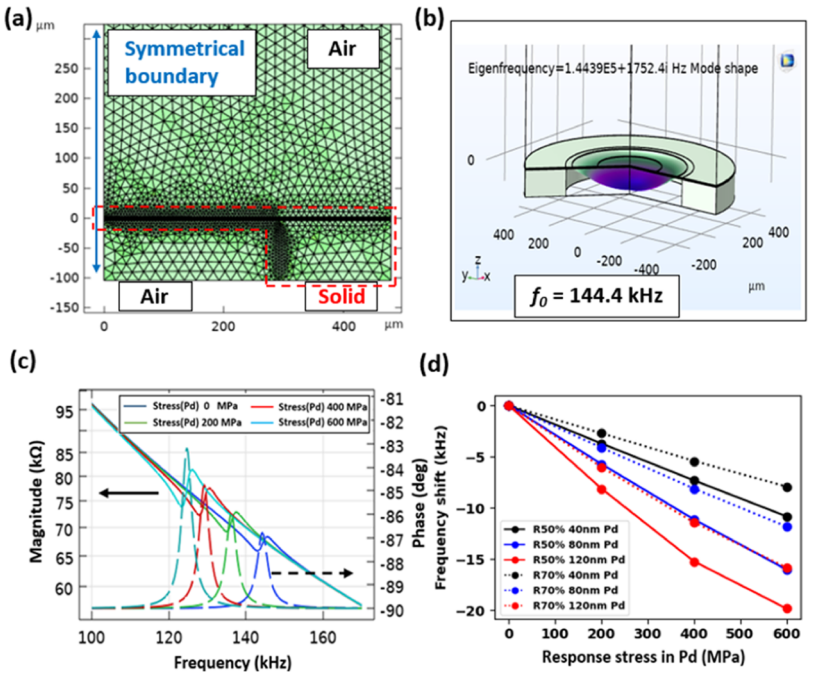

Figure 3. Simulation results of (a) meshing map and physic situation. (b) Eigenfrequency of PMD device and the mode shape. (c) Impedance magnitudes and phases change with compressive stress in Pd film for R70% 120 nm Pd coating device. (d) Frequency response of Pd stress change for PMD devices with various thicknesses of Pd coating.

MODEL AND EXPERIMENT

Sensor Design. The PMD sensor comprises two primary components: a bottom PMD resonator and a top Pd sensing layer, as illustrated in Figure 1a.

The PMD resonator's structure is carefully engineered for optimal performance. It features a piezoelectric stack of 1-μm-thick $Sc_{0.15}Al_{0.85}N$, chosen for its minimal ferroelectric hysteresis and long-term piezoelectric stability,[19,20] sandwiched between two 0.2-μm-thick molybdenum (Mo) electrodes. A 4-μm-thick epitaxial silicon elastic layer underneath enhances effective transverse driving efficiency by maintaining the neutral axis away from the piezoelectric stack,[21] while providing appropriate structural flexibility for high response sensitivity. A 0.5-μm-thick silicon nitride (Si_3N_4) + undoped silicate glass (USG) isolation layer covers the piezoelectric stack for protection. The resonator is built on a patterned substrate with a 585 μm diameter etched through the cavity on the backside aimed for an ~150 kHz resonant frequency. Electrical connectivity between the top (signal) and bottom (ground) electrodes is facilitated through vias and aluminum metal routing.

This study employs devices with 50% (R50%) and 70% (R70%) piezoelectric stack-to-cavity diameter covering ratios, as shown in Figure 1b,c respectively, both before and after Pd coating with a 90% diameter-to-cavity covering ratio. These design variations enable comprehensive analysis for precise H_2 gas molecule detection while optimizing the PMD resonator's performance.

Sensor Working Principle. The sensor's working principle hinges on the Pd sensing layer's interaction with ambient H_2 molecules as depicted in Figure 2. This interaction disrupts interatomic forces within the Pd film,[22] causing lattice expansion and inducing compressive stress that transforms the flat elastic diaphragm into a convex shape. The Pd−H_2 interaction progresses dynamically from physisorption to deep chemisorption as H_2 concentration increases, with 1% H_2 potentially inducing ~600 MPa of compressive stress in the 50 nm sensing film.[23]

Crucially, the PMD's eigenfrequency is proportional to the square root of diaphragm stress as shown in eq 1.[24] This relationship enables H_2 concentration prediction through measured eigenfrequency shifts, effectively converting the H_2 concentration into a detectable mechanical response and subsequent frequency change.

$$\Delta f_{01} \propto \frac{\gamma_{01}}{4\pi\sqrt{\rho\sigma_r}}\Delta\sigma_r \tag{1}$$

where Δf_{01} is the resonant frequency shift, γ_{01} is the flexible mode constant, σ_r is the average stress of the diaphragm, and ρ is the diaphragm density.

Simulation. Comprehensive COMSOL FEM simulations were conducted to theoretically analyze the PMD sensor's resonance frequency response to sensing layer stress, as shown in Figure 3a. To optimize the computational efficiency, a 2D symmetrical model was employed, incorporating key interfaces of solid structures and surrounding acoustic media. The analysis combined eigenfrequency and frequency domain studies, ensuring consistency and validation. Figure 3b,c presents the critical findings: For example, a PMD device with 50% covering ratio and 120-nm-thick Pd coating (R50% 120 nm Pd) exhibited a 144.4 kHz resonant frequency under flexible vibration mode. Notably, as the Pd sensing layer's response stress increases from 0 to 600 MPa, the device's impedance resonant peak shifts from 144.4 to 124.2 kHz, demonstrating a clear correlation between stress and frequency response.

Figure 3d illustrates the comparative stress sweep simulations for various Pd sensing layer thicknesses (40, 80, and 120 nm) on both R50% and R70% devices. The results reveal a clear trend in sensitivity: the R50% device with a 120 nm Pd

https://doi.org/10.1021/acssensors.4c03069
ACS Sens. 2025, 10, 1922−1929

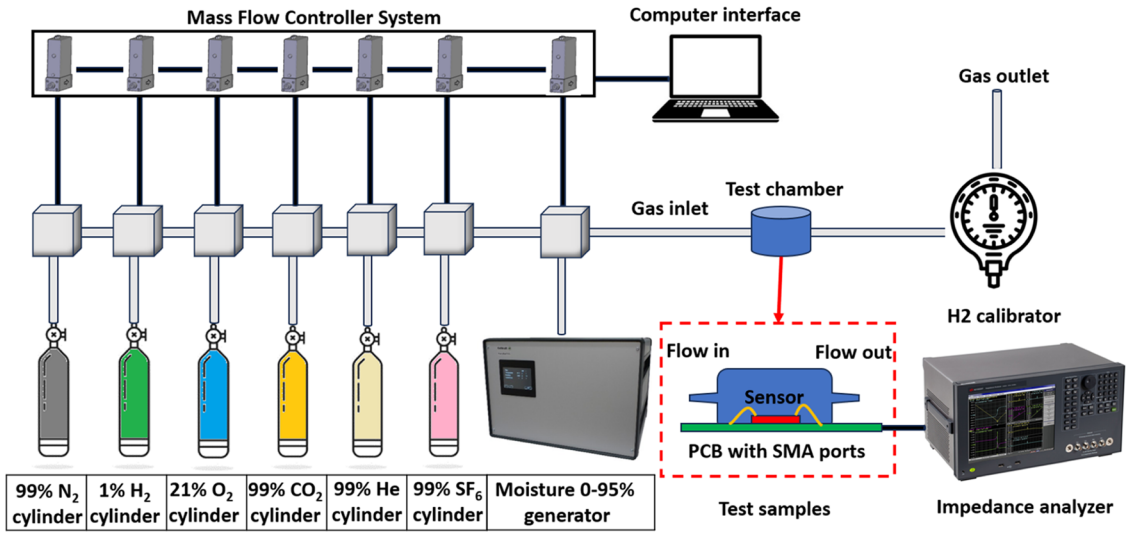

Figure 4. Experimental test setup schematic and related instruments.

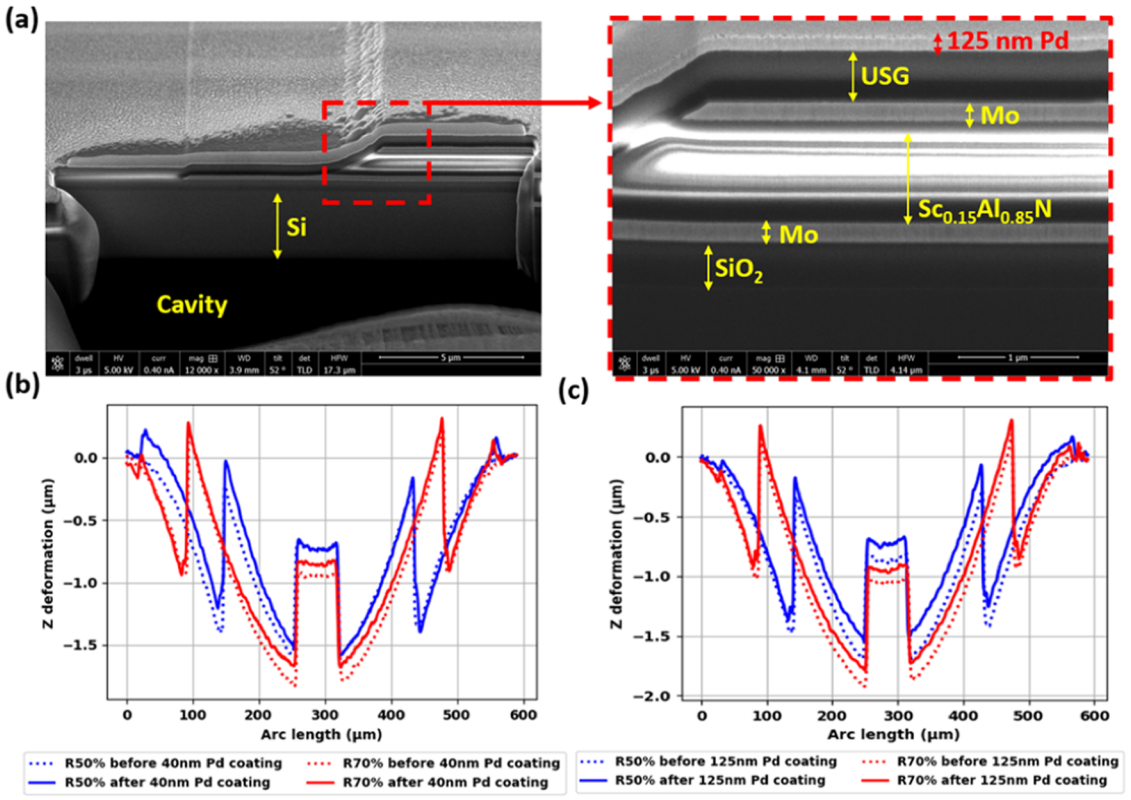

Figure 5. Pd film coating characterizations of (a) oblique angle SEM image after FIB cutting on the PMD electrode edge step area and its zoom-in view. (b) Optical profile of PMD sensors before and after 40 nm Pd coating. (c) Optical profile of PMD sensors before and after 125 nm Pd coating.

layer exhibited the highest sensitivity at 20.2 kHz per 600 MPa (equivalent to 20.2 kHz/% H_2), while the R70% device with a 40 nm Pd layer showed the lowest sensitivity at 7.7 kHz per 600 MPa (7.7 kHz/% H_2). This pattern suggests two key design principles for optimizing sensor sensitivity: (1) a smaller piezoelectric stack covering ratio and (2) a thicker Pd coating. These findings provide valuable guidance for enhancing the H_2 response sensitivity potentially leading to more accurate H_2 detection capabilities.

H_2 Test Setup. The experimental test setup, displayed in Figure 4, comprises three main components: a gas control system, a test chamber, and data processing equipment. The gas control system features gas source cylinders (N_2, H_2, O_2, CO_2, He, and SF_6), a Cellkraft Humidifier P-2 moisture generator, and corresponding mass flow meters controlled via computer interface software. This system enables precise gas combinations at a 1000 sccm flow rate for H_2 response, moisture, and cross-sensitivity tests, with N_2 serving as the default carrier gas. The test chamber consists of a 3D-printed

https://doi.org/10.1021/acssensors.4c03069
ACS Sens. 2025, 10, 1922−1929

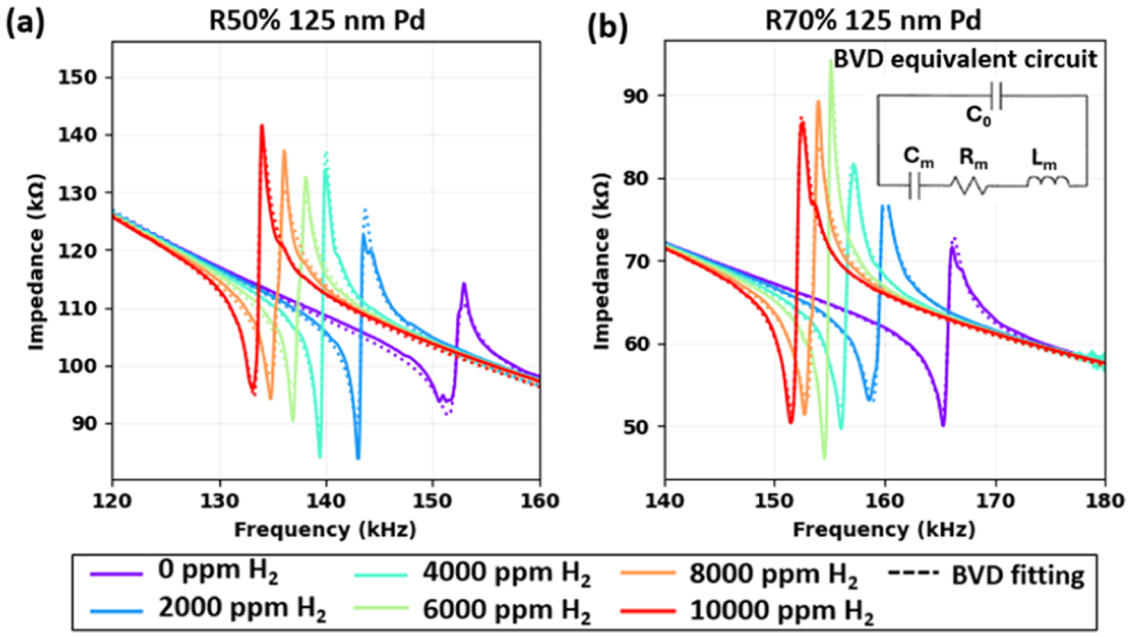

Figure 6. Impedance spectrum characterizations for (a) the R50% 125 nm Pd device and (b) the R70% 125 nm Pd device under various H_2 concentrations and the corresponding BVD equivalent circuit fitting.

Table 1. BVD Equivalent Circuit Fitting Extraction Parameters for PMD R50% and R70% 125 nm Pd Sensors

	PMD R50% 125 nm Pd device							PMD R70% 125 nm Pd device						
H_2 (ppm)	f_0 (kHz)	Q	K_t^2 (%)	C_0 (pF)	C_m (pF)	R_m (kΩ)	L_m (H)	f_0 (kHz)	Q	K_t^2 (%)	C_0 (pF)	C_m (pF)	R_m (kΩ)	L_m (H)
0	152.1	104.3	0.24	10.40	0.020	499.4	54.5	165.6	160.3	0.27	15.63	0.034	176.6	27.2
2000	143.3	185.2	0.23	10.39	0.020	303.9	62.5	159.4	141.3	0.34	15.57	0.043	163.4	23.1
4000	139.7	235.2	0.24	10.39	0.020	239.0	64.1	156.4	158.1	0.36	15.57	0.046	140.4	22.6
6000	137.4	116.2	0.32	10.39	0.027	370.8	49.9	154.8	268.2	0.33	15.58	0.041	93.3	25.7
8000	135.4	105.7	0.34	10.39	0.029	387.7	48.2	153.4	141.9	0.41	15.57	0.052	140.6	20.7
10 000	133.6	158.5	0.31	10.39	0.026	291.6	55.1	151.9	168.0	0.40	15.57	0.050	124.8	22.0

plastic cap with gas inlet and outlet ports, attached to a PCB where the PMD sensor chip is mounted and wire-bonded for electrical connectivity. Throughout all experiments, an impedance analyzer measures the PMD sensor's impedance spectrum, while a Model GPA2000 H_2 calibrator ensures accurate H_2 concentration calibration.

RESULTS AND DISCUSSION

Sensor Structure Characterization. Pd film coating characterization was conducted using scanning electron microscopy (SEM) coupled with focused ion beam (FIB) cutting on the piezoelectric stack edge of devices with three different Pd thicknesses, as shown in Figure 5a. The measured Pd film thicknesses were 39.4, 84.6, and 125.0 nm, respectively, each within a ± 5.0 nm error range. Optical surface profiles before and after Pd coating for R50% and R70% devices, presented in Figure 5b,c, respectively, reveal crucial insights into the PMD devices' structural characteristics and stress dynamics. Notably, R70% devices, with their larger piezoelectric stack covering ratio, exhibit approximately 0.4 μm greater concave deformation compared to R50% devices, indicating the dominance of tensile residual stress from the piezoelectric stack in determining initial deformation. The nearly identical initial states observed in devices with the same ratio underscore the excellent uniformity achieved in the fabrication process. Furthermore, the consistent deformation status before and after Pd coating for each device suggests that the addition of 40−125 nm pure Pd film does not significantly alter the devices' mechanical stress state. These observations collectively highlight the robustness of the fabrication process and the minimal impact of Pd coating on the initial stress state, providing valuable understanding of the PMD devices' behavior with varying Pd coating thicknesses.

Sensor H_2 Characterization. Impedance spectrum characterization of PMD sensors was conducted under H_2 concentrations ranging from 0 to 10 000 ppm, with results for R50% and R70% devices (125 nm Pd coating) demonstrated in Figure 6a,b, respectively. As H_2 concentration increases, both device types exhibit a leftward shift in resonant peak, with R50% devices showing a more pronounced shift compared with R70% devices. Notably, both device types display robust electrical signals across the full H_2 response range, enabling accurate processing through a Butterworth-Van Dyke (BVD) equivalent circuit fitting. This fitting achieved excellent match quality (R^2 > 99%), allowing for reliable extraction of key parameters, which are compiled in Table 1 for precise data analysis.

Analysis of the extracted key parameters in Table 1 reveals significant differences between PMD R50% and R70% devices with a 125 nm Pd coating. The R50% device, with its smaller piezoelectric stack covering ratio, exhibits a resonant frequency of 152.1 kHz, which is 13.5 kHz lower than the R70% device. This lower frequency is attributed to reduced stiffness and less impact from piezoelectric stack residual stress. Apparently, the

https://doi.org/10.1021/acssensors.4c03069
ACS Sens. 2025, 10, 1922−1929

R50% device demonstrates superior H_2 sensitivity, with a frequency sensitivity of 18.5 kHz/%, 1.35 times higher than that of the R70% device. Conversely, the R70% device shows better electrical performance, with an average Q factor 15% higher and a K_t^2 value 25% higher than that of the R50% device. These findings highlight a trade-off between the smaller and larger piezoelectric stack devices: smaller piezoelectric stacks offer higher sensitivity but relatively lower electrical signal quality.

The H_2 sensitivities of PMD R50% and R70% devices with Pd coating thicknesses ranging from 40 to 125 nm are illustrated in Figure 7 revealing several key trends. For the same Pd thickness, R50% devices consistently demonstrate 1.2−1.35 times higher sensitivity than R70% devices, while increasing Pd coating thickness by a factor of 1 within the same piezoelectric stack ratio results in a 1.4−1.6 times sensitivity increase. Moreover, all devices exhibit higher sensitivity in the low H_2 concentration range (0−2000 ppm), with limit of detection at ∼50 ppm. Experimental results align well with simulation trends, with the PMD R50% device with 125 nm Pd coating showing the highest sensitivity at 18.5 kHz/%, and the PMD R70% device with 40 nm Pd coating exhibiting the lowest sensitivity at 6.5 kHz/%. Both simulation and experimental results confirm that R50% devices with thicker Pd coatings demonstrate sensitivity approximately 3 times higher compared to R70% devices with thinner Pd coatings. These findings underscore the significant impact of both piezoelectric stack ratio and Pd coating thickness on H_2 sensor sensitivity, providing crucial insights for better PMD sensor design.

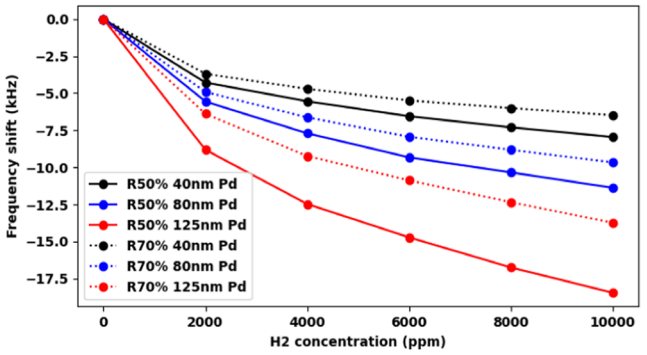

Figure 7. PMD H_2 sensor sensitivity of R50% and R70% devices with 40−125 nm thickness of Pd coating.

Figure 8 illustrates the response time characteristics of PMD H_2 sensors with Pd coating thicknesses ranging from 40 to 125 nm. The 40 nm Pd coating device demonstrates rapid performance, with an average 90% absorption response time of only 41 s and a 90% desorption response time of 547 s. As the thickness of the Pd sensing layer increases, a counterbalancing effect emerges: while response sensitivity improves, both absorption and desorption response times are extended. This relationship can be attributed to the properties of thicker Pd films, which offer larger H_2 storage capacity and higher saturation thresholds. Since H_2 gas molecule penetration occurs primarily through the surface area, increasing Pd thickness while maintaining the same penetration rate results in longer saturation times. Consequently, thicker Pd films require more time to reach equilibrium during both the absorption and desorption processes, despite their enhanced sensitivity.

Robustness to humidity is a critical concern for most resonant sensors due to its potential impact on frequency response through mass changes.[25] To address this, humidity response tests were conducted on PMD R50% devices, with the results presented in Figure 9a. Remarkably, the frequency shifts for all devices remained within ±0.26 kHz across a wide humidity range of 0−80% RH, demonstrating robust performance under varying moisture conditions.

Furthermore, cross-sensitivity characterization was performed on the PMD R50% device with a 125 nm Pd coating, as illustrated in Figure 9b. The sensor was sequentially exposed to 99.9% N_2, 21% O_2, 20% CO_2, 20% He, 20% SF_6, and back to 99.9% N_2 gas, with each exposure lasting 10 min. Throughout the 36 min continuous test, the observed frequency shift remained below ±0.25 kHz, indicating excellent selectivity toward H_2 and minimal interference from other common gases. These results underscore the PMD sensor's resilience to humidity variations and its high specificity for H_2 detection, crucial attributes for reliable operation in diverse environmental conditions.

Table 2 summarizes the comparison between the PMD H_2 sensor developed in this work and the existing resonant H_2 sensors. Unlike other resonant frequency-based sensors that rely on the Sauerbrey mass-loading equation, where sensitivity is primarily dependent on working frequency, the PMD sensor

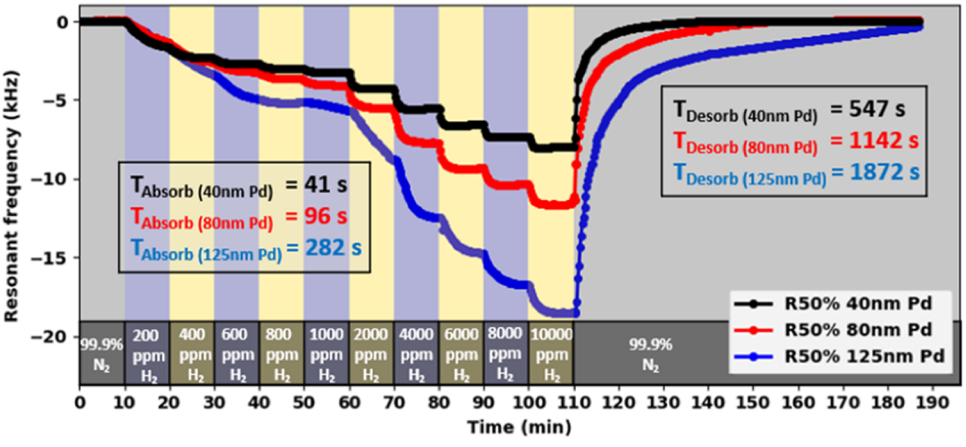

Figure 8. H_2 response time characterization for PMD R50% 40−125 nm devices.

https://doi.org/10.1021/acssensors.4c03069
ACS Sens. 2025, 10, 1922−1929

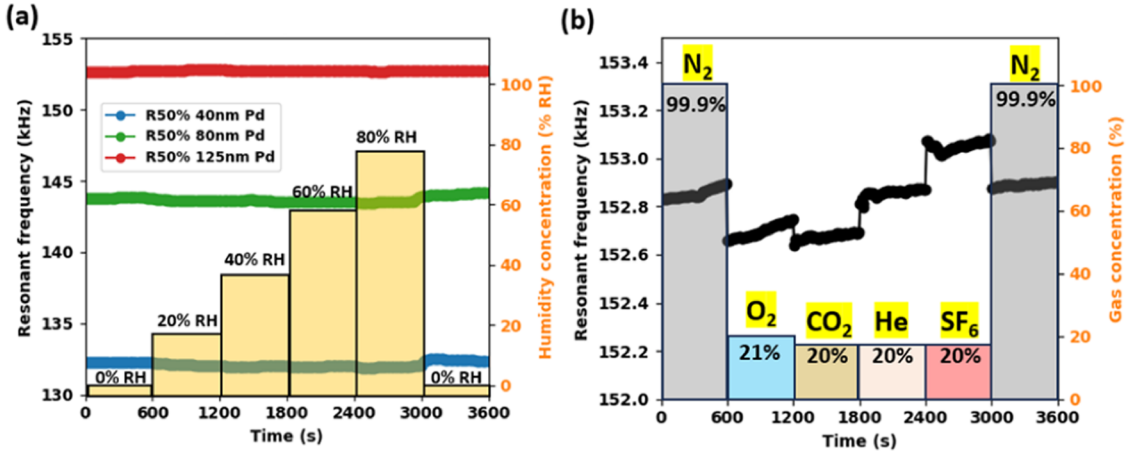

Figure 9. Selectivity characterization for (a) humidity response of PMD R50% 40−125 nm devices. (b) Cross-sensitivity characterization for PMD R50% 125 nm device.

Table 2. Comparison of PMD H_2 Sensor with Existing Resonant H_2 Sensors

based resonator types	sensing materials	working frequency (MHz)	detect range (%)	sensitivity (kHz/%)	T_{absorb}/T_{desorb} (s)	FOM (ppm/%)	lateral size (μm)	signal quality	ref
FBAR	Pd	2230	0−2	5000	40/70	2.2×10^3	500	high Q	7
FBAR	ZnO	2390	0−3	6100	20/40	2.6×10^3	500	high Q	8
SAW	Pd/Cu	150	0−1	1.5	4/4	1.0×10^1	3200	low Q	9
SAW	Pt/ZnO	129	0−1	55	60/120	4.3×10^2	6000	low Q	10
QCM	g-C_3N_4	9	2−20	2.5×10^{-3}	200/250	2.8×10^{-1}	5000	mid Q	11
QCM	Pd	165	0−0.025	∼5.3	∼29/-	3.2×10^1	1800	mid Q	12
PMD	Pd (40 nm)	0.13	0−1	8.0	41/547	6.2×10^4	600	mid Q	this work
	Pd (125 nm)	0.15		18.5	282/1872	1.2×10^5			

operates on a stress-based mechanism. Despite functioning at a significantly lower resonant frequency of 150 kHz (1000 times lower than SAW sensors), the PMD sensor achieves a similar level absolute sensitivity of 18.5 kHz/%. Significantly, the FOM for the PMD sensor reaches 10^5, substantially surpassing other H_2 resonant sensors. With a compact lateral length of only 600 μm, similar to FBAR dimensions, the PMD sensor is well suited for IC integration. While the response time is currently determined by the sensing material, it offers potential for further optimization through Pd alloy and nano surface structure design.[13−15]

CONCLUSIONS

This work presents a novel PMD H_2 sensor that significantly advances the field of resonant frequency-based H_2 sensing. By uniquely integrating a PMD resonator with a Pd sensing layer, we have developed a sensor that operates on a stress-based mechanism, diverging from mass-loading principles. This innovative approach enables the sensor to achieve an unprecedented FOM exceeding 1×10^4, substantially outperforming existing resonant H_2 sensors. Despite operating at a relatively low frequency of 150 kHz, the PMD sensor demonstrates a remarkable sensitivity of 18.5 kHz/% H_2, comparable to high-frequency SAW sensors. With a lateral span of just 600 μm, the sensor exhibits a form factor conducive to facile IC integration. Comprehensive characterization, including impedance spectrum analysis, H_2 sensitivity measurements, and cross-sensitivity tests, confirms the sensor's excellent performance, with a low limit of detection of 50 ppm and minimal interference from humidity and other gases. While the response time, determined by Pd thickness, presents a trade-off with sensitivity, it offers the potential for further optimization through material engineering. These results underscore the PMD sensor's potential to revolutionize H_2 detection across various applications, combining high sensitivity, compact size, and robust performance in a single device.

AUTHOR INFORMATION

Corresponding Authors

Jihang Liu − *Institute of Microelectronics (IME), Agency for Science, Technology and Research (A*STAR), Singapore 138634, Republic of Singapore;* orcid.org/0000-0002-6690-8711; Email: Liujh4@ime.a-star.edu.sg

Yao Zhu − *Institute of Microelectronics (IME), Agency for Science, Technology and Research (A*STAR), Singapore 138634, Republic of Singapore;* orcid.org/0000-0002-1582-0816; Email: zhuya@ime.a-star.edu.sg

Authors

Doris Keh Ting Ng − *Institute of Microelectronics (IME), Agency for Science, Technology and Research (A*STAR), Singapore 138634, Republic of Singapore;* orcid.org/0000-0001-9178-4987

Yul Koh − *Institute of Microelectronics (IME), Agency for Science, Technology and Research (A*STAR), Singapore 138634, Republic of Singapore*

Subhranu Samanta − *Institute of Microelectronics (IME), Agency for Science, Technology and Research (A*STAR), Singapore 138634, Republic of Singapore*

https://doi.org/10.1021/acssensors.4c03069
ACS Sens. 2025, 10, 1922−1929

Weiguo Chen − *Institute of Microelectronics (IME), Agency for Science, Technology and Research (A*STAR), Singapore 138634, Republic of Singapore*
Md Hazwani Khairy Md Husni − *Institute of Microelectronics (IME), Agency for Science, Technology and Research (A*STAR), Singapore 138634, Republic of Singapore*
Merugu Srinivas − *Institute of Microelectronics (IME), Agency for Science, Technology and Research (A*STAR), Singapore 138634, Republic of Singapore*
Qingxin Zhang − *Institute of Microelectronics (IME), Agency for Science, Technology and Research (A*STAR), Singapore 138634, Republic of Singapore*
Fuu Ming Kai − *National Metrology Centre (NMC), Agency for Science, Technology and Research (A*STAR), Singapore 637145, Republic of Singapore*
Peter Hyun Kee Chang − *Institute of Microelectronics (IME), Agency for Science, Technology and Research (A*STAR), Singapore 138634, Republic of Singapore*

Complete contact information is available at: https://pubs.acs.org/10.1021/acssensors.4c03069

Notes

The authors declare no competing financial interest.

■ ACKNOWLEDGMENTS

This research was supported by the National Research Foundation, Singapore, and A*STAR (Agency for Science, Technology and Research), Singapore under its Low-Carbon Energy Research (LCER) Funding Initiative (FI) (Award No. U2102d2012) for fabrication (sensing layer deposition and patterning) and testing; it is also support by A*STAR under its Industry Alignment Fund—Industry Collaboration Projects (IAF-ICP), with Grant No. I2301E0027, Project Title: Piezo Specialty Lab-in-Fab 2.0 (LiF 2.0) for fabrication of piezoelectric micro diaphragm (PMD).

■ REFERENCES

(1) Darmadi, I.; Nugroho, F. A. A.; Langhammer, C. High-Performance Nanostructured Palladium-Based Hydrogen Sensors - Current Limitations and Strategies for Their Mitigation. *ACS Sens.* **2020**, *5* (11), 3306−3327.
(2) Abdel-Aal, H. K.; Sadik, M.; Bassyouni, M.; Shalabi, M. A New Approach to Utilize Hydrogen as a Safe Fuel. *Int. J. Hydrogen Energy* **2005**, *30* (13−14), 1511−1514.
(3) Cui, B.; Ren, Z.; Wang, W.; Cheng, L.; Gao, X.; Huang, L.; Hu, A.; Hu, F.; Jin, J. Review of Surface Acoustic Wave-Based Hydrogen Sensor. *Sens. Actuators Rep.* **2024**, *7*, 100197 DOI: 10.1016/j.snr.2024.100197.
(4) Addabbo, T.; Fort, A.; Mugnaini, M.; Tani, M.; Vignoli, V.; Bruzzi, M. Quartz Crystal Microbalance Sensors Based on TiO2 Nanoparticles for Gas Sensing. In *2017 IEEE International Instrumentation and Measurement Technology Conference (I2MTC)*; IEEE, 2017; pp 1−6.
(5) Vinita; Pareek, D.; Masiul Islam, S.; Singh, J. Bulk Acoustic Wave Resonators for Sensing Applications: A Review. *Sens. Actuators, A* **2024**, *378*, No. 115839.
(6) Liu, J.; Zhao, Z.; Fang, Z.; Liu, Z.; Zhu, Y.; Du, L. High-Performance FBAR Humidity Sensor Based on the PI Film as the Multifunctional Layer. *Sens. Actuators, B* **2020**, *308*, No. 127694.
(7) Chen, D.; Wang, J. J.; Li, D. H.; Xu, Y. Hydrogen Sensor Based on Pd-Functionalized Film Bulk Acoustic Resonator. *Sens. Actuators, B* **2011**, *159* (1), 234−237.
(8) Chen, D.; Wang, J. J.; Liu, Q. X.; Xu, Y.; Li, D. H.; Liu, Y. J. Highly Sensitive ZnO Thin Film Bulk Acoustic Resonator for Hydrogen Detection. *J. Micromech. Microeng.* **2011**, *21* (11), 115018 DOI: 10.1088/0960-1317/21/11/115018.
(9) Wang, W.; Liu, X.; Mei, S.; Jia, Y.; Liu, M.; Xue, X.; Yang, D. Development of a Pd/Cu Nanowires Coated SAW Hydrogen Gas Sensor with Fast Response and Recovery. *Sens. Actuators, B* **2019**, *287*, 157−164.
(10) Phan, D. T.; Chung, G. S. Surface Acoustic Wave Hydrogen Sensors Based on ZnO Nanoparticles Incorporated with a Pt Catalyst. *Sens. Actuators, B* **2012**, *161* (1), 341−348.
(11) Ishiguro, Y.; Nishitani, T.; Li, C.; Hirakuri, K. A Graphitic Carbon Nitride-Coated Quartz Crystal Microbalance Gas Sensor for H2 Detection. *J. Mater. Chem. C* **2023**, *11* (30), 10178−10184.
(12) Zhou, L.; Kato, F.; Nakamura, N.; Oshikane, Y.; Nagakubo, A.; Ogi, H. MEMS Hydrogen Gas Sensor with Wireless Quartz Crystal Resonator. *Sens. Actuators, B* **2021**, *334*, 129651.
(13) Kilinc, N.; Sanduvac, S.; Erkovan, M. Platinum-Nickel Alloy Thin Films for Low Concentration Hydrogen Sensor Application. *J. Alloys Compd.* **2022**, *892*, No. 162237.
(14) Rane, S.; Arbuj, S.; Rane, S.; Gosavi, S. Hydrogen Sensing Characteristics of Pt−SnO2 Nano-Structured Composite Thin Films. *J. Mater. Sci. Mater. Electron.* **2015**, *26* (6), 3707−3716.
(15) Lee, S.; Kang, Y.; Lee, J.; Kim, J.; Shin, J. W.; Sim, S.; Go, D.; Jo, E.; Kye, S.; Kim, J.; An, J. Atomic Layer Deposited Pt Nanoparticles on Functionalized MoS2 as Highly Sensitive H2 Sensor. *Appl. Surf. Sci.* **2022**, *571*, No. 151256.
(16) Gehin, C.; Barthod, C.; Teisseyre, Y. Design and Characterisation of a New Force Resonant Sensor. *Sens. Actuators, A* **2000**, *84* (1), 65−69.
(17) Liu, J.; Chen, D. S.; Jian, G. D.; Choong, D.; Wai, S.; Srinivas, M.; Huamao, L.; Xin, Z. Q.; Chang, P.; Kee, H.; Giusti, D.; Leotti, A.; Ercoli, F. D.; Lazzari, C.; Tacchini, R.; Koh, Y. Residual Stress Analysis in ScAlN Micro- Diaphragm for High Sensitivity and Wide Range Pressure Sensing. In *2024 IEEE Ultrasonics, Ferroelectrics, and Frequency Control Joint Symposium (UFFC-JS)*; IEEE, 2024; pp 1−4.
(18) Olfatnia, M.; Xu, T.; Ong, L. S.; Miao, J. M.; Wang, Z. H. Investigation of Residual Stress and Its Effects on the Vibrational Characteristics of Piezoelectric-Based Multilayered Microdiaphragms. *J. Micromech. Microeng.* **2010**, *20* (1), 015007 DOI: 10.1088/0960-1317/20/1/015007.
(19) Choong, D. S. W.; Goh, D. J.; Liu, J.; Merugu, S.; Zhang, Q. X.; Lee, H. K.; Chang, P.; Leotti, A.; Tan, H. S.; Magbujos, V.; Hur, Y. J.; Lin, H.; Chadnra Rao, B. S. S.; Ghosh, S.; Ramegowda, P. C.; Chen, D. S. H.; Giusti, D.; Quaglia, F.; Ng, E. J.; Lee, J. E. Y. Correlation of Wafer-Scale Film Stress Effects on ScAlN PMUT Parameters. In *2022 IEEE International Ultrasonics Symposium (IUS)*; IEEE, 2022; pp 1−4.
(20) Liu, J.; Jian, G. D.; Chen, D. S.; Choong, D.; Wai, S.; Shyam, T.; Ramegowda, C.; Srinivas, M.; Huamao, L.; Xin, Z. Q.; Chang, P.; Kee, H.; Das, A.; Sciarrone, A.; Leotti, A.; Giusti, D.; Lee, J. E.; Koh, Y. Towards Unparallelled CMOS-Compatible Air-Coupled PMUT Performance with 30% Sc-Doped AlN through an Analysis of Residual Stress Effects. In *2024 IEEE Ultrasonics, Ferroelectrics, and Frequency Control Joint Symposium (UFFC-JS)*; IEEE, 2024; pp 1−4.
(21) Lu, Y.; Horsley, D. A. Modeling, Fabrication, and Characterization of Piezoelectric Micromachined Ultrasonic Transducer Arrays Based on Cavity SOI Wafers. *J. Microelectromech. Syst.* **2015**, *24* (4), 1142−1149.
(22) Lee, H. S.; Kim, J.; Moon, H.; Lee, W. Hydrogen Gas Sensors Using Palladium Nanogaps on an Elastomeric Substrate. *Adv. Mater.* **2021**, *33* (47), 2005929.
(23) McKeown, S. J.; Wang, X.; Yu, X.; Goddard, L. L. Realization of Palladium-Based Optomechanical Cantilever Hydrogen Sensor. *Microsyst. Nanoeng.* **2017**, *3* (1), 1−6.
(24) Olfatnia, M.; Xu, T.; Miao, J. M.; Ong, L. S.; Jing, X. M.; Norford, L. Piezoelectric Circular Microdiaphragm Based Pressure Sensors. *Sens. Actuators, A* **2010**, *163* (1), 32−36.
(25) Hallil, H.; Dejous, C.; Hage-Ali, S.; Elmazria, O.; Rossignol, J.; Stuerga, D.; Talbi, A.; Mazzamurro, A.; Joubert, P. Y.; Lefeuvre, E. Passive Resonant Sensors: Trends and Future Prospects. *IEEE Sens. J.* **2021**, *21* (11), 12618−12632.